HHS Public Access

Author manuscript

Nat Neurosci. Author manuscript; available in PMC 2016 January 01.

Published in final edited form as:

Nat Neurosci. 2015 July ; 18(7): 997–1007. doi:10.1038/nn.4037.

Distinct circuit-dependent functions of presynaptic neurexin-3 at GABAergic and glutamatergic synapses

Jason Aoto[1,*], **Csaba Földy**[1], **Silviana Maria Ciurea Ilcus**[1], **Katsuhiko Tabuchi**[1,2,3], and **Thomas C. Südhof**[1,2]

[1]Dept. of Molecular and Cellular Physiology, Stanford University Medical School, 265 Campus Drive, CA 94305-5453, USA

[2]Howard Hughes Medical Institute, Stanford University Medical School, 265 Campus Drive, CA 94305-5453, USA

[3]Division of Cerebral Structure, Department of Cerebral Research, National Institute for Physiological Sciences, Okazaki, Japan

Abstract

α- and β-neurexins are presynaptic cell-adhesion molecules whose general importance for synaptic transmission is well documented. The specific functions of neurexins, however, remain largely unknown because no conditional neurexin knockouts are available, and because targeting all α- and β-neurexins produced by a particular gene is challenging. Using newly-generated constitutive and conditional knockout mice that target all neurexin-3α and -3β isoforms, we here show that neurexin-3 is differentially required for distinct synaptic functions in different brain regions. Specifically, we find that in cultured neurons and acute slices of the hippocampus, presynaptic neurexin-3 mediates trans-synaptic regulation of postsynaptic AMPA-receptors via its extracellular sequences. In cultured neurons and acute slices of the olfactory bulb, however, presynaptic neurexin-3 is selectively required for GABA release by a mechanism involving its intracellular sequences. Thus, our data demonstrate that neurexin-3 performs distinct essential pre- or postsynaptic functions in different brain regions by distinct mechanisms.

Keywords

synaptic cell-adhesion; synapse formation; synaptic transmission; neurexins; AMPA-receptors; olfactory bulb; olfactory circuit

[*]Address for correspondence: jaoto@stanford.edu (J.A.); Tel.: 650-721-1421; Fax: 650-498-4585.

J.A., K.T. and T.C.S. conceived the project. K.T. generated the *Nrxn3α/β*cKO mice and performed biochemical analyses of protein expression. J.A. designed and performed all immunocytochemistry, culture and acute hippocampal slice electrophysiology and animal behavior experiments. J.A. and C.F. performed olfactory bulb acute slice analyses. J.A. and T.C.S. wrote and edited the manuscript.

INTRODUCTION

Synapse formation and maintenance require precise coordination between pre- and postsynaptic neurons to produce the properties characteristic of a particular type of synapse. This coordination is thought to be mediated by trans-synaptic cell-adhesion molecules such as neurexins, which are evolutionarily conserved presynaptic proteins that bind to multiple postsynaptic ligands[1–4].

Vertebrates express three neurexin genes (*Nrxn1*, *Nrxn2*, and *Nrxn3* in mice), each of which encodes longer α- and shorter β-neurexins[5–7] (Fig. 1a). Human *NRXN1* mutations are associated with autism and schizophrenia[8–11], and *NRXN3* mutations are linked to addiction and obesity[12–17]. Extensive alternative splicing of neurexins at six canonical sites (SS#1–SS#6) creates thousands of neurexin isoforms[18,19] (Fig. 1a). α- and β-neurexins and their various splice variants display a differential regional expression pattern in brain, such that most neurons express multiple α- and β-neurexins in different combinations[19,20].

Constitutive KO mice of individual α-neurexins are viable and fertile, whereas double and triple α-neurexin KO mice are lethal, likely due to impaired synaptic function[21]. Moreover, using knockin (KI) mice expressing *Nrxn3* at normal levels but either always with or without an insert in SS#4, we showed that Nrxn3 alternative splicing at SS#4 controls basal and activity-dependent postsynaptic AMPA-receptor (AMPAR) levels in the hippocampus[20]. However, to date no studies examined the overall functions of all α- and β-neurexins encoded by an individual gene. In this regard it is interesting that invertebrates express only α-neurexin isoforms that also appear to perform essential synaptic functions, although different studies have suggested diverse, and sometimes-contradictory roles[22,23].

Here, we generated conditional KO mice ablating all α- and β-forms of *Nrxn3*, arguably the best studied neurexin isoform[20]. We examined the *Nrxn3α/β* KO phenotypes in the hippocampus and olfactory bulb, and directly compared these phenotypes to those of the *Nrxn3α/β* SS#4 KI and of the *Nrxn3α* KO mice. Our data reveal that in hippocampus, presynaptic *Nrxn3α/β* KO phenocopied the *Nrxn3α/β* SS#4 KI, suggesting that trans-synaptic regulation of postsynaptic AMPARs is the major essential function of Nrxn3 in the hippocampus. In olfactory bulb, by contrast, presynaptic *Nrxn3α/β* KO revealed an essential role in enabling presynaptic GABA release. Moreover, rescue using Nrxn3 mutants demonstrated that the presynaptic release phenotype in olfactory bulb neurons required intracellular Nrxn3 sequences, whereas the postsynaptic AMPAR-level changes in hippocampal neurons did not. These results suggest that Nrxn3 is differentially essential for distinct functions mediated by diverse mechanisms in different neural circuits; consistent with the notion that differential expression of various neurexin isoforms in different types of neurons shapes the synaptic properties.

RESULTS

Conditional and constitutive *Nrxn3α/β* KO mice

We used homologous recombination in mouse ES cells to flank the first common exon for *Nrxn3*α and *Nrxn3β* (exon 18 [5]) with loxP sites (Fig. 1b). Following the deletion of exon

18 by cre recombinase, the resulting mRNA contains a frame-shift in the sixth LNS-domain. If the mutant mRNAs were sufficiently stable to still produce protein, such protein would be C-terminally misfolded and lack a membrane anchor, rendering it non-functional. Thus, we refer to the floxed *Nrxn3* allele as a conditional KO (cKO) allele.

When we converted the conditional *Nrxn3*α/β KO mice into constitutive *Nrxn3α/β* KO mice by cre-mediated germline recombination, we found that most homozygous *Nrxn3*α/β KO mice died at birth (Fig. 1c). Surviving homozygous constitutive *Nrxn3*α/β KO mice were runted and exhibited ataxia and hyperactivity when examined on a force plate actometer[24] (Figs. 1d & 1e). However, no major changes in protein composition were noted (Supplementary Figs. 1a and 1b). Thus, constitutive *Nrxn3*α/β KO mice exhibit a significant overall phenotype that is more severe than that of *Nrxn3*α KO and *Nrxn3*α/β SS#4 KI mice[20,21], prompting us to explore the consequences of *Nrxn3α/β* ablation on synaptic function.

Deletion of *Nrxn3α/β* but not of *Nrxn3α* alone in cultured hippocampal neurons selectively impairs AMPAR-mediated synaptic transmission

To analyze *Nrxn3*α/β function in precisely matching mutant and control neurons while avoiding the lethality of constitutive *Nrxn3*α/β KO mice, we cultured hippocampal neurons from newborn homozygous *Nrxn3*α/β cKO mice. We infected the neurons with lentiviruses expressing inactive (control) or active cre-recombinase (cre) fused to EGFP, and examined the neurons by whole-cell patch-clamp recordings two weeks later.

We first measured spontaneous ‘minis’ (miniature excitatory and inhibitory postsynaptic currents [mEPSCs and mIPSCs, respectively]; Figs. 2a–d). We found that the *Nrxn3*α/β deletion did not change mEPSC and mIPSC mini frequencies, but produced a dramatic decrease in mEPSC amplitude, while the mIPSC amplitude was unaffected. The loss of *Nrxn3α/β* did not alter passive membrane properties or mEPSC and mIPSC kinetics (Supplementary Figs. 2a–c). The selective decrease in mEPSC amplitude in *Nrxn3*α/β cKO neurons mirrors the phenotype we previously observed in hippocampal *Nrxn3*α/β SS#4 KI neurons which express only the *Nrxn3*α/β SS#4 variant containing an insert in SS#4[20].

We next examined the effect of the conditional *Nrxn3*α/β KO on evoked synaptic transmission. We observed a specific and selective ~50% decrease in AMPAR- but not in NMDAR-mediated excitatory responses or in GABAergic inhibitory responses (Figs. 2e–2g). The reduction in mEPSC amplitude and selective decrease in AMPAR- but not NMDAR-mediated synaptic transmission indicates that the *Nrxn3α/β* cKO impairs postsynaptic AMPAR levels but does not alter presynaptic glutamate release. To test if *Nrxn3*α/β cKO regulates presynaptic release probability at excitatory synapses, we measured the paired-pulse ratio of NMDAR-mediated EPSCs and the progressive, activity-dependent, blockade of NMDAR-mediated EPSCs induced by the open-channel blocker MK-801 (Fig. 2h, Supplementary Fig. 2d). Both approaches provide sensitive but indirect assessments of the presynaptic release probability[25–28], but revealed no changes induced by acute deletion of *Nrxn3*α/β.

Does Nrxn3α alone reproduce the *Nrxn3α/β* cKO phenotype? We cultured hippocampal neurons from littermate *Nrxn3α*$^{+/+}$ and constitutive *Nrxn3*α$^{-/-}$ mice. We detected no significant change in passive membrane properties or mEPSC amplitude or frequency (Supplementary Fig. 2e & 2f). Moreover, evoked EPSCs mediated by AMPARs or NMDARs were unaltered by the constitutive *Nrxn3*α KO, as were paired-pulse ratios of NMDAR-mediated EPSCs (Supplementary Figs. 2g–i). Thus, *Nrxn3*β must have the capacity to functionally compensate for the loss of *Nrxn3α* in the hippocampus of *Nrxn3*α KO mice.

*Nrxn3*α/β deletion decreases surface AMPAR levels and enhances GluA1 internalization

The unexpected similarity in phenotypes between the *Nrxn3*α/β KO and the *Nrxn3*α/β SS#4 KI prompted us to ask whether these electrophysiological phenotypes are mediated by the same biological mechanisms.

To address this question, we live surface labeled *Nrxn3α/β* cKO neurons infected with inactive or active cre-recombinase using antibodies against the extracellular N-terminus of GluA1. We then fixed and permeabilized the GluA1 labeled neurons, and immunostained them for the excitatory pre- and postsynaptic markers vGluT1 and PSD-95, respectively (Figs. 3a–d, Supplementary Figs. 3a–c). The puncta densities representing GluA1, vGluT1 or PSD95 were unchanged between control and *Nrxn3*α/β-deficient neurons, consistent with a normal synapse density (Fig. 3b). However, GluA1-immunoreactive surface puncta sizes were reduced ~50% in *Nrxn3*α/β KO neurons, whereas vGluT1- and PSD95-positive puncta sizes were unchanged. as were the intensities (signal strength per unit area) of GluA1-, vGluT1- or PSD95-positive puncta (Figs. 3c & 3d, Supplementary Figs. 3a & 3b). In parallel experiments, we quantified the surface levels of GluA2, and observed a ~50% reduction in surface puncta size without significant changes in puncta density or intensity (Figs. 3a–3d, Supplementary Figs. 3a–c) Thus, total surface levels of AMPARs are selectively decreased in *Nrxn3*α/β-deficient neurons compared to control neurons. This specific reduction in GluA1 and GluA2 surface immunoreactivity is likely not due to a reduction in total AMPAR levels because the total protein levels of GluA1 and GluA2 in constitutive *Nrxn3*α/β KO animals was not detectably changed (Supplementary Figs. 1a & 1b).

To test how acute deletion of *Nrxn3*α/β decreases postsynaptic surface AMPAR levels, we measured basal GluA1 internalization[20,39]. We incubated *Nrxn3*α/β cKO neurons expressing inactive or active cre-recombinase with an antibody raised against the extracellular N-terminus of GluA1 for 5 min, followed by a 15–20 min chase to allow partial internalization of surface-labeled GluA1. We fixed the neurons without permeabilization, and labeled them with an Alexa-488 (green) conjugated secondary antibody to detect the uninternalized population of surface GluA1, and subsequently permeabilized the neurons and labeled them with a different Alexa-546 (red) conjugated secondary antibody to detect the internalized fraction of GluA1. As a control, non-permeabilized neurons displayed no red immunofluorescence signal, indicating that the first secondary antibody, AlexaFluor488, completely saturated the surface population of labeled GluA1 (Fig. 3e).

We found that the *Nrxn3*α/β KO increased the GluA1 internalization (measured as the internalized/total fluorescence) by ~60% relative to control neurons (Figs. 3e & 3f; Supplementary Fig. 3d). Thus, the genetic ablation of *Nrxn3*α/β destabilizes the surface levels of postsynaptic GluA1-containing AMPARs presumably via a trans-synaptic interaction, independent of excitatory synapse formation.

This phenotype is strikingly similar to that of Nrxn3α/β KI neurons constitutively expressing Nrxn3α/β$^{SS\#4+}$, suggesting that the primary, non-redundant Nrxn3α/β function in hippocampus is to maintain normal postsynaptic AMPAR levels, which is critically dependent on the expression of the Nrxn3α/β$^{SS\#4-}$ isoform.

Both α- and β-neurexins rescue hippocampal *Nrxn3α/β* KO phenotype

We next asked whether the decrease in postsynaptic AMPAR levels in *Nrxn3*α/β KO neurons reflects a general function of neurexins that depends on SS#4, and whether this activity is specific for Nrxn3α or Nrxn3β. To address these questions, we performed rescue experiments in cultured hippocampal neurons.

Both *Nrxn3*α and *Nrxn3*β rescued the *Nrxn3α/β* KO phenotype, but only when they lacked an insert at SS#4 (Figs. 4a & b). To define the minimal properties of Nrxn3 required to mediate postsynaptic AMPAR function, we attempted to rescue the phenotype with mutant Nrxn3. The extracellular domain of Nrxn3α without the splice-site #4 insert, anchored to the membrane via a GPI anchor was sufficient to restore AMPAR-mediated transmission to wild-type levels (Fig. 4c). Whereas the GPI anchored Nrxn3α SS#4− extracellular domain succeeded in stabilizing AMPAR transmission, a soluble *Nrxn3*β variant – resulting from a SS#5 insert containing an early stop codon[5] – failed to rescue the *Nrxn3*α/β KO phenotype (Fig. 4d, Supplementary Fig. 4a). We found that *Nrxn1β* and *Nrxn2β* without an insert in SS#4 also rescued the *Nrxn3*α/β KO phenotype, demonstrating the potential for splice-site #4 dependent functional redundancy among neurexins (Fig. 4e). Moreover, when the Nrxn1β transmembrane region and cytoplasmic tail were exchanged for those of the unrelated PDGF receptor was still fully capable of rescue (Fig. 4f, Supplementary Fig. 4b). These experiments define the fundamental neurexin characteristics necessary for controlling postsynaptic AMPARs, demonstrating that neurexins lacking an insert at SS#4 can redundantly rescue the conditional *Nrxn3*α/β KO phenotype without requiring their intracellular sequences, suggesting that neurexin-mediated trans-synaptic interactions stabilize postsynaptic AMPARs in cultured hippocampal neurons independent of neurexin-mediated intracellular signaling.

Presynaptic *Nrxn3*α/β $^{SS\#4-}$ acts trans-synaptically on AMPARs by binding to a postsynaptic neurexin ligand, likely LRRTM2[20]. To assess if the same mechanism applies for the *Nrxn3*α/β KO phenotype, we took two separate approaches. First, we tested whether postsynaptic deletion of *Nrxn3*α/β in isolated neurons produced the same phenotype as the *Nrxn3α/β* deletion in all neurons. We sparsely transfected primary hippocampal cultures from *Nrxn3*α/β cKO mice with EGFP fused to inactive (control) or active cre-recombinase (cre), which exhibit strict nuclear localization, and performed whole-cell patch-clamp recordings from neurons with EGFP+ nuclei, but found no change in AMPAR-mediated synaptic responses (Fig. 4g). Second, we infected all *Nrxn3*α/β cKO neurons in a culture

dish with lentiviruses expressing inactive or active cre-recombinase, and then asked if sparse postsynaptic co-transfection of *Nrxn3*β without the SS#4 insert and cytoplasmic EGFP could rescue the *Nrxn3*α/β KO phenotype. We identified transfected versus untransfected neurons by intense cytoplasmic EGFP fluorescence and found that postsynaptic rescue did not restore AMPAR-mediated synaptic responses (Fig. 4h). Together, these experiments support the notion that presynaptic *Nrxn3* is required to stabilize postsynaptic AMPA-receptors and to enable AMPAR-mediated synaptic transmission.

Our current findings, together with previous data on *Nrxn3*α/β SS#4 KI neurons[20], thus suggest that Nrxn3^{SS4-} isoforms perform a dominant and essential active function in retaining postsynaptic AMPARs in hippocampal cultures. This function is lost either when only Nrxn3^{SS4+} is expressed, or when *Nrxn3*α/β is deleted entirely. Furthermore, our findings suggest that extracellular Nrxn3 sequences, anchored to the presynaptic plasma membrane and lacking an insert at SS#4, are necessary and sufficient to trans-synaptically stabilize postsynaptic AMPARs. However, all of these observations were made *in vitro* in developing cultured hippocampal neurons, prompting us to ask whether *Nrxn3α/β* performs a similar function in adult hippocampal neurons *in vivo*.

Presynaptic deletion of *Nrxn3α/β in vivo* at CA1-subiculum synapses impairs postsynaptic AMPAR-mediated responses

We stereotactically injected adeno-associated viruses (AAVs) expressing active or inactive Cre-recombinase fused to EGFP into the CA1 region of *Nrxn3α/β* cKO mice at P21 and analyzed AMPAR-mediate transmission at CA1-subiculum synapses on P35-42. We first confirmed that our injection coordinates largely confined the AAV infection to the CA1 region with minimal spillover into the adjacent subiculum (Fig. 5a). Using horizontally cut slices (300 μm thickness), we stimulated CA1 afferents with an extracellular stimulating electrode in the stratum oriens/alveus at the CA1-subiculum border, and recorded from uninfected postsynaptic subicular neurons (Fig. 5b). The subiculum is populated by two types of pyramidal neurons, identified by their intrinsic firing properties as burst- and regular-firing neurons (Supplementary Fig. 5a and b). We observed a significant reduction in AMPAR input-output relationship without a change in presynaptic release probability or intrinsic membrane properties in both types of neurons (Figs. 5c–f; Supplementary Figs. 5c & d). These results confirm that the primary role of presynaptic *Nrxn3α/β* in the hippocampus *in vivo* is to stabilize postsynaptic AMPARs at mature synapses.

Nrxn3 is required for presynaptic GABA release in olfactory bulb neurons independent of SS#4

Our results thus far reveal only one essential function of *Nrxn3*α/*β* in hippocampal neurons: to trans-synaptically maintain postsynaptic AMPAR levels. These results do not rule out SS#4-independent *Nrxn3*α/β functions that are otherwise masked in hippocampal neurons due to redundant expression of other neurexins,. Since neurexins are known to be differentially expressed in brain regions[19,20], we reasoned that it may be possible to unmask other *Nrxn3*α/β functions by analyzing other types of neurons in which compensating neurexin expression may be reduced. We focused on the olfactory bulb because previous

studies found that olfactory bulb neurons express *Nrxn3*α^{SS4+} at particularly high levels[19,20].

We cultured olfactory bulb neurons from homozygous *Nrxn3*α/β cKO mice and infected the neurons with lentiviruses encoding inactive (control) or active cre-recombinase (cre) (Fig. 6a). *Nrxn3*α/β-deficient olfactory bulb neurons did not exhibit changes in excitatory or inhibitory synapse morphology (Fig. 6b; Supplementary Fig. 6a – c). We next patched large mitral/tufted cells and measured mEPSC frequency and amplitude. Surprisingly in view of the results in hippocampus (Fig. 2), we detected no change (Fig. 6c, Supplementary Figs. 6d & e). We also examined evoked AMPAR- and NMDAR-mediated EPSCs as well as the excitatory presynaptic release probability, and observed no change in *Nrxn3α/β* cKO neurons (Fig. 6d – f). Thus, in olfactory bulb synapses *Nrxn3*α/β is not essential for excitatory synaptic transmission.

The lack of an effect of the *Nrxn3α/β* cKO on AMPARs in olfactory bulb neurons prompted us to ask whether the previously observed correlation between Nrxn3α/β function and alternative splicing at SS#4 in Nrxn3α/β also applies to the olfactory bulb. We examined if the experimental manipulation of Nrxn3 SS#4 would result in an excitatory transmission phenotype in olfactory bulb neurons, but detected none (Figs. 6g – j, Supplementary Figs. 6f & g). This result appears to confirm the correlation between the functions of Nrxn3α/β and its alternative splicing at SS#4.

We next tested inhibitory synaptic transmission. In contrast to the hippocampus, we observed a marked reduction in mIPSC frequency (~40%), but not in mIPSC amplitude or mIPSC kinetics in *Nrxn3*α/β-deficient olfactory bulb neurons (Fig. 7a, Supplementary Figs. 7a & b). We detected a large reduction (~60%) in the amplitude of evoked IPSCs in *Nrxn3*α/β KO neurons (Fig. 7b). The decreased mIPSC frequency and evoked IPSC amplitude in *Nrxn3*α/β KO neurons could be explained by a smaller readily-releasable pool (RRP) of GABA-containing synaptic vesicles, or by impaired coupling of an action potential to GABA release. To test these hypotheses, we first measured IPSCs evoked by an application of 0.5 M hypertonic sucrose, which monitors the size of the RRP of synaptic vesicles[28], but observed no change in RRP size (Supplementary Fig. 7c). However, the conditional ablation of *Nrxn3α/β* resulted a large increase in IPSC PPR, consistent with a decrease in release probability (Fig 7c). These data suggest that *Nrxn3*α/β deletion decreases GABAergic transmission in cultured olfactory bulb neurons – in which granule cells make up the vast majority of GABAergic neurons – by decreasing the efficacy with which an action potential triggers GABA release from granule cells.

Does Nrxn3α/β function in GABA release from olfactory bulb neurons depend on both Nrxn3α and Nrxn3β, and is it regulated by Nrxn3α/β alternative splicing at SS#4 similar to the Nrxn3α/β function in stabilizing postsynaptic AMPARs in hippocampal neurons? To address these questions, we analyzed inhibitory synaptic transmission in olfactory bulb neurons (1) cultured from littermate *Nrxn3α*$^{+/+}$ or *Nrxn3α*$^{-/-}$ mice, and (2) cultured from homozygous *Nrxn3α/β* SS#4 KI mice, infected with lentiviruses expressing inactive (which retains the SS#4+ genotype) or active cre-recombinase (which generates the SS#4− genotype).

The constitutive ablation of *Nrxn3α* phenocopied the GABA release phenotype observed in *Nrxn3*α/β cKO cultured olfactory bulb neurons, suggesting that only Nrxn3α is essential for GABA release in granule cell neurons (Fig. 7d–f, Supplementary Fig. 7d and 7e). Conversely, we observed that SS#4 alternative splicing had no effect on inhibitory synaptic transmission in cultured olfactory bulb neurons (Figs. 7g–i, Supplementary Figs. 7f and 7g). Together, these data suggest that different from the hippocampus, where Nrxn3 is essential for postsynaptic retention of AMPARs via the redundant action of both Nrxn3α and Nrxn3β in a manner regulated by SS#4 alternative splicing, in olfactory bulb Nrxn3 is required for presynaptic GABA release primarily via the action of Nrxn3α in a manner independent of SS#4 alternative splicing. In other words, these results suggest that Nrxn3α/β has brain region-specific pre- and postsynaptically manifesting functions that are mediated by distinct mechanisms.

Nrxn3α function in GABA release from olfactory bulb neurons requires its intracellular sequences

We asked whether the extracellular sequences of Nrxn3 are sufficient for its function in maintaining normal GABA release in olfactory bulb neurons, similar to their role in retaining postsynaptic AMPARs (Fig. 4c). We tested whether GABA release probability in olfactory bulb neurons could be restored by full-length Nrxn3α^{SS4+} or by truncated Nrxn3α^{SS4+} that is tethered to the presynaptic plasma membrane via a GPI-anchor (Supplementary Figs. 7h and 7i). We performed these rescue experiments using Nrxn3α with an insert in SS#4 to match the endogenous isoform expression found in the olfactory bulb[20].

Full-length Nrxn3α^{SS4+} fully rescued evoked IPSCs, demonstrating that the direct genetic manipulation of *Nrxn3* directly affects GABAergic release probabilities (Fig. 7j & k). Strikingly, GPI-anchored Nrxn3α failed to rescue the GABA release phenotype (Fig. 7l & m), despite its ability to localize to the synapse and restore AMPAR-mediated synaptic transmission in hippocampal neurons (Fig. 4c). Thus, in contrast to the hippocampus where the SS#4-dependent precise identity of trans-synaptic interactions is sufficient and necessary to stabilize excitatory transmission, these data establish that in olfactory bulb, the initiation of Nrxn3-dependent trans-synaptic interactions alone is not sufficient to regulate presynaptic release but also requires the intracellular sequences of *Nrxn3*.

In vivo olfactory bulb ablation of *Nrxn3* impairs GABAergic synaptic transmission and olfaction

To examine whether *Nrxn3*α/β in adult olfactory bulb neurons functions *in vivo* in a similar capacity as in developing cultured olfactory bulb neurons, we bilaterally stereotactically injected AAVs expressing inactive (control) or active cre-recombinase (cre) fused to EGFP into the granule cell layer of *Nrxn3α/β* cKO olfactory bulbs at P21 (Fig. 8a–c). 14–21 days after injections, we cut 300 μm horizontal olfactory bulb slices,,placed an extracellular stimulating electrode in the lateral olfactory tract (LOT), and evoked granule cell-mediated IPSCs by antidromic stimulation of mitral cell axons, while recording in whole-cell voltage-clamp mode from uninfected postsynaptic mitral cells in the mitral cell layer (Fig. 8c and Supplemental Fig. 8a). Consistent with our findings in culture, we observed a striking

reduction in GABAergic synapse strength measured by a large impairment in the IPSC input-output relationship following the loss of *Nrxn3*α/β in granule cells (Fig. 8d).

To determine if the reduction in local inhibition in the olfactory bulb circuit following conditional ablation of *Nrxn3*α/β in adult mice resulted in a behavioral change, we subjected the mice to a buried food-finding assay. Previous reports have demonstrated that the disruption of granule cell-dependent inhibitory transmission alters olfactory discrimination and impairs food-finding behavior[29]. We found that the deletion of *Nrxn3*α/β from the majority of inhibitory granule cells increased the latency to find buried food relative to animals infected with control AAVs, confirming the functional importance of the role of Nrxn3α/β in inhibitory synaptic transmission in the olfactory bulb (Fig. 8e, Supplementary Fig. 8b).

DISCUSSION

Here, we generated conditional *Nrxn3α/β* KO mice using a strategy that ablates all α- and β-Nrxn3 forms, analyzed the phenotypes induced by constitutive or conditional KO of all Nrxn3 forms at multiple levels, and compared these phenotypes to those produced by the constitutive *Nrxn3α* KO[21], and the conditional *Nrxn3 SS#4* KI that allows control of SS#4 alternative splicing with normal Nrxn3α/β expression levels[20]. We examined two brain regions, the hippocampus and the olfactory bulb, by electrophysiology and immunocytochemistry using cultured neurons that were infected with cre-recombinase expressing lentiviruses *in vitro*, or acute slices/tissue sections that were obtained from mice after stereotactic infections with cre-recombinase expressing AAVs *in vivo*. Our results identified two major, non-redundant synaptic functions of Nrxn3α/β: Nrxn3α/β was selectively required for maintaining normal postsynaptic AMPAR levels in the hippocampus, whereas, it was selectively essential for controlling the presynaptic release probability at inhibitory synapses in the olfactory bulb (Supplementary Table 1).

The *Nrxn3α/β* cKO AMPAR phenotype observed in the hippocampus is very similar to that of *Nrxn3α/β* SS#4 KI mice that express *Nrxn3α/β* at normal levels but with a constitutively included insert in SS#4[20]. In the *Nrxn3α/β* SS#4 KI mice, the phenotype can be rescued simply by excising the SS#4 insert; accordingly, we found that the *Nrxn3α/β* cKO phenotype could be rescued only by neurexins without an insert in SS#4, but not with an insert in SS#4 (Fig. 3 and Supplementary Table 1). Moreover, both in Nrxn3α/β KO and in Nrxn3α/β SS#4 KI neurons the AMPAR impairment was rescued by a C-terminally truncated version of Nrxn3α or Nrxn3β in which its extracellular sequences (without an insert at SS#4) were tethered to the presynaptic plasma membrane by an unrelated sequence (Fig. 3)[20]. Thus, the hippocampal phenotypes of both the *Nrxn3α/β* cKO and the constitutive *Nrxn3α/β* SS#4 KI are likely a direct result of disrupting trans-synaptic Nrxn3-ligand interactions (likely with LRRTMs) which serve to anchor AMPARs at the synapse and suggest that the predominant essential function of Nrxn3α/β in excitatory hippocampal synapses is to mediate presynaptic, SS#4-dependent regulation of postsynaptic AMPARs, which is surprising considering the many ligands and functions that are generally associated with neurexins. Moreover, these results raise the fundamental question whether alternative splicing of other neurexins at SS#4 also plays similarly critical functions, and whether the

lack of the AMPAR-related phenotype in Nrxn3α/β-deficient olfactory bulb neurons may be due to the compensating functions of other, correctly alternatively spliced neurexins in these neurons.

In contrast to the postsynaptic phenotype of Nrxn3α/β-deficient hippocampal neurons, the presynaptic release phenotype we observed in olfactory bulb neurons is consistent with previous notions of neurexin functions as organizers of the presynaptic release machinery[21]. Specifically, our results suggest that in inhibitory olfactory bulb neurons (likely granule cells where Nrxn3α is predominantly expressed[19]), Nrxn3α/β functions to maintain evoked GABA release. The interpretation that the decrease in inhibitory synaptic strength in olfactory bulb neurons is due to a decrease in the Ca^{2+}-dependent release is based on the decrease in mIPSC frequency and the severe change in PPR observed in the *Nrxn3α/β* KO neurons, without a change in the readily-releasable pool size. Since the GABA release phenotype was similarly observed in olfactory bulb neurons lacking only Nrxn3α, Nrxn3β clearly does not functionally compensate in inhibitory olfactory bulb synapses likely due to the undetectable/low levels of *Nrxn3β* expression in granule cells[19]. Moreover, since the GABA release phenotype in Nrxn3α/β-deficient neurons could not be rescued by a membrane-tethered Nrxn3α construct lacking the intracellular Nrxn3α sequences, Nrxn3α is likely essential for normal GABA release via an action mediated by its cytoplasmic tail. Intriguingly, we failed to observe excitatory postsynaptic changes in Nrxn3α/β-deficient olfactory bulb neurons, and we detected no effect of alternative splicing of Nrxn3α/β at SS#4 on the Nrxn3α release function. Together, these findings indicate that Nrxn3 cell-autonomously governs presynaptic release probability in inhibitory olfactory bulb neurons. It remains to be established whether this Nrxn3 function also requires its extracellular sequences and involves trans-synaptic interactions as well as intracellular signaling, and if so, what postsynaptic neurexin ligands that bind to both SS#4 isoforms may be involved.

How is it possible that the same gene (*Nrxn3α/β*) performs two distinct, non-overlapping functions in two different brain regions and at two different types of synapses? This very observation illustrates the intriguing yet confounding layers of molecular and functional redundancy and complexity of neurexins. This observation can most plausibly be explained by the finding that different types of neurons and different brain regions express distinct patterns of neurexins (both in terms of principal isoforms and splice variants) and of neurexin ligands (of which there are many, ranging from postsynaptic cell-adhesion molecules to secreted proteins). Since neurexins exhibit a high degree of sequence homology, they are likely redundant for their central functions, but may additionally perform isoform-specific functions. Moreover, α- and β-neurexins share many sequences including the LNS6 domain which is the minimal extracellular domain required for binding to most known neurexin ligands as well as the entire intracellular sequences, and might provide an explanation for some but not all functions. Thus, different patterns of expression of neurexin variants and of neurexin ligands will result in distinct patterns of essential vs. redundant functions for a given neurexin gene. Genetic manipulations can only unmask functions that are not redundant with other genes, and the two very different functions of Nrxn3α/β we here describe could therefore be the simple consequence of differential patterns of expression of redundant other neurexins and of postsynaptic ligands. For

example, if hippocampal neurons expressed lower levels of Nrxn1$^{SS\#4-}$ and Nrxn2$^{SS\#4-}$ than Nrxn3$^{SS\#4-}$ but similar absolute levels of all three neurexins, a release function mediated by all three neurexins may not be apparent in these neurons even when the AMPAR-maintenance function becomes manifest. Conversely, if olfactory bulb neurons expressed significant levels of Nrxn1β$^{SS\#4-}$ or Nrxn2β$^{SS\#4-}$ but these β-neurexins were unable to sustain GABA release, loss of Nrxn3α/β would cause a selective GABA release phenotype, but not an AMPAR-related phenotype.

Our current findings provide systematic and comprehensive insight into *Nrxn3α/β* function at excitatory and inhibitory synapses in two distinct brain regions. To our knowledge, this is the first study to systematically analyze the effects of different mutations in the same gene (*Nrxn3*) in different brain regions using conditional manipulations. Our findings illustrate the multifarious fundamental functions of neurexins, and strengthen the notion that the circuit-level consequences associated with disease-relevant genetic abnormalities in neurexins must be addressed in a cell type-specific context.

METHODS

Mouse generation and husbandry

Nrxn3αβ cKO mutant mice were generated by homologous recombination in R1 embryonic stem cells using the strategy outlined in Fig. 1b. The *Nrxn3αβ* cKO mouse line was obtained after flp-recombinase-mediated germ line deletion of the neo cassette. The *Nrxn3α β*constitutive KO mouse line was produced by cre-recombinase mediated deletion of exon 18 in the germ line of *Nrxn3α β*cKO mutant mice by breeding to a CMV-cre line[34]. The *Nrxn3α* KO and Nrxn3^{SS4+} mouse lines were previously described[20,21]. All animal are maintained in a hybrid genetic background consisting of C57/B6 × Sv/129 and housed on a 12hr light/dark cycle. All animals studies were approved by the Stanford animal use committees, and all original mouse lines were deposited in Jackson Labs for distribution.

mRNA measurements

Validation of genetic manipulation of exon excision was performed on mRNA isolated from DIV14 primary hippocampal cultures infected with inactive (control) or active cre-recombinase (cre). qRT-PCR reactions were performed in triplicates for each condition (150ng total RNA) with 2× VeriQuest master-mix (Affymetrix) and gene-specific qRT-PCR probes (IDT DNA). Reactions were run on a 7900HT Fast RT-PCR instrument (Applied Biosystems). mRNA from single Mitral/Tufted or inhibitory granule cells was isolated from primary olfactory bulb cultures and neurexin expression profiles were generated using Fluidigm BioMark (Fluidigm). Briefly, cytoplasm from single neurons was aspirated into patch electrodes and immediately snap-frozen in 2× cells-direct buffer (Invitrogen). Single-cell RNA was then pre-amplified for 18 cycles using gene specific primers to the target genes of interest. For internal controls (not shown), total RNA was also isolated from P21 olfactory bulbs was purified using the TriZol method (Invitrogen), and pre-amplified together with the single cell samples. Critical threshold cycles (Ct) values were then determined by using custom designed Taqman assays and BioMark48×48 Dynamic Array integrated fluidic circuit (Fluidigm), and the resulting data were analyzed by custom made

scripts in Mathematica 9 (Wolfram Research). The data are plotted as normalized expression relative to β-actin.

DNA constructs

Inactive and active cre-recombinase viral constructs for lentivirus and adeno-associated virus production were previously described[20]. Briefly, inactive and active cre recombinase constructs are engineered to express EGFP fusion proteins that are localized to the nucleus. Full-length Nrxn1, Nrxn2, and Nrxn3 SS#4+/− rescue constructs have been described previously[20]. All constructs were cloned from whole brain cDNA isolated from C57/B6 mice and primers were designed against the appropriate sequences[5] and subcloned into the lentiviral plasmid, FSW.

Electrophysiology in primary culture

Electrophysiological measurements were performed in DIV14-16 primary neurons cultured from the hippocampus or olfactory bulbs of newborn *Nrxn3αβ* cKO, *Nrxn3α* KO or Nrxn3^{SS4+} mice. *Nrxn3α/β* cKO and Nrxn3^{SS4+} neuronal cultures were infected with lentivirus on DIV3-4 that expressed either inactive (control; Nrxn3^{SS4+}) or active (cre; Nrxn3^{SS4-}) cre-recombinase. Rescue experiments in *Nrxn3α/β* cKO neurons were performed by concurrent superinfection with rescue viruses. Whole-cell patch-clamp recordings were performed in cultured neurons at DIV13-16 as described[29,34]. Cultures were continuously superfused with extracellular solution (ACSF; in mM): 126 NaCl, 2.5 KCl, 1 NaH_2PO_4, 26.2 $NaHCO_3$, 2.5 $CaCl_2$, 1.3 $MgSO_4$-$7H_2O$, 11 D-Glucose, ~290 mOsm. Excitatory and inhibitory currents (mEPSCs/EPSCs and mIPSCs/IPSCs) were recorded from excitatory pyramidal neurons (hippocampal culture) and larger mitral/tufted cells (olfactory bulb culture) with 3–4 MΩ pipettes (WPI) filled with an internal solution containing the following (in mM): 119 Cesium-Methanesulfonate, 15 CsCl, 8 NaCl, 10 TEA-Cl, 0.2 EGTA, 4 Na_2-ATP, 0.3 Na_2-GTP, 10 HEPES, 10 Phosphocreatine at pH 7.3 with CsOH, ~300 mOsm. A constant hyperpolarizing current was used to maintain a resting potential of –60 to –70 mV. mEPSCs and mIPSCs were recorded in the presence of 0.5 μM tetrodotoxin (TTX) plus either 100 μM picrotoxin (mEPSCs) or 10 μM 6-cyano-7-nitroquinoxaline-2,3-dione (CNQX) and 50 μM D-(−)-2-amino-5-phosphonopentanoic acid (D-APV) (mIPSCs), respectively. Miniature events were visually inspected, individually selected and analyzed in Clampfit 10 (Molecular Devices) using template matching and an amplitude threshold of 5 pA. Evoked synaptic currents were examined as previously described[35–37]. Briefly, a bipolar stimulating electrode, made with nichrome wire (A-M Systems, Carlsborg, WA), placed at a position 100–150 μm from the soma of recorded neurons triggered evoked synaptic currents. After the formation of the whole-cell configuration and equilibrium of the intracellular pipette solution, the series resistance was compensated to 5–8 MΩ. To isolate individual glutamatergic and GABAergic currents, evoked responses were recorded in the presence of 100 μM picrotoxin and 50 μM D-APV (AMPAR), and 10 μM CNQX (NMDAR), and 10 μM CNQX and 50 μM D-APV (IPSCs). Presynaptic release probability was monitored by measurements of the paired-pulse ratios at inter-stimulus intervals ranging from 40 ms – 400 ms. For evoked release experiments, 10 μM QX-314 (final concentration) was added to the internal solutions and dialyzed into postsynaptic neurons to prevent firing.

Electrophysiology in acute slices

Electrophysiological recordings from acute hippocampal slices from Nrxn3α/β cKO animals injected with AAVs expressing GFP fused to inactive (control) or active (cre) cre-recombinase on P21 were performed as previously described[20]. Briefly, on P35-42, 300 μm horizontal brain slices were cut in a high sucrose cutting solution (in mM): 85 NaCl, 75 sucrose, 2.5 KCl, 1.3 NaH_2PO_4, 24 $NaHCO_3$, 0.5 $CaCl_2$, 4 $MgCl_2$ and 25 D-Glucose and allowed to recover in ACSF at 31°C for 30 min followed by a hour at room temperature. To record AMPAR input-output current, a nichrome stimulating electrode was placed at the most distal portion of CA1 in the Stratum Oriens/alveus. Postsynaptic AMPAR currents were measured in burst and regular spiking neurons in the subiculum. The identity of the postsynaptic neuron was determined in whole-cell current clamp mode using an internal that consisted of (in mM): 140 K-gluconate, 5 KCl, 10 HEPES, 4 ATP-Mg_2, 0.5 GTP-Na_2, 10 phosphocreatine and 0.2 EGTA. After identification of subicular neuron cell-type, the AMPAR input-output relationship was measured in whole-cell voltage clamp mode. AMPAR paired-pulse ratios were performed at ISIs ranging from 20 ms – 400 ms. All recordings in the hippocampus were performed in the presence of 100 μM D-APV and 100 μM picrotoxin.

Slice electrophysiology from olfactory bulb preparations were performed as previously described[29]. Briefly, olfactory bulbs were stereotactically injected on P21 and prepared for recording on P35-42. 300mm horizontal slices were made from the olfactory bulb in the same sucrose-based cutting solution described above and allowed to recover as described. To evoke granule cell-mediated IPSC current, a nichrome stimulating electrode was placed in the lateral olfactory tract. Uninfected (GFP negative) mitral/tufted cells, located in the mitral cell layer of the olfactory bulb, were subjected to whole cell voltage clamp recordings. The internal solution for these experiments consisted of (in mM): 119 Cesium-Methanesulfonate, 15 CsCl, 8 NaCl, 10 TEA-Cl, 0.2 EGTA, 4 Na_2-ATP, 0.3 Na_2-GTP, 10 HEPES, 10 Phosphocreatine at pH 7.3 with CsOH, ~300 mOsm.

Data was collected at 10 kHz and filtered with a lowpass filter at 2 kHz. The frequency, duration, and magnitude of the extracellular stimulus was controlled by a Model 2100 Isolated Pulse Stimulator (A-M Systems, Inc.) synchronized with the Clampex 10 data acquisition software (Molecular Devices). For all electrophysiological experiments, the experimenter was blind to the recording condition.

Production of recombinant lentivirus for primary culture

Lentiviruses were produced as previously described[34]. Lentiviral transfer vectors were co-transfected with third-generation helper plasmids (VSVG, pRSV-REV, and pMDLg/pRE) into HEK293T cells by calcium phosphate transfection. Viral particles were harvested 48 hours after transfection, spun at 500 × g for 5 minutes to pellet cellular debris, and added to cultured neurons.

Production of recombinant Adeno-Associated Viruses for *in vivo* injection

AAV-DJ expressing GFP fused to inactive or active cre-recombinase was generated as previously described[20]. Briefly, HEK293T cells were co-transfected with the AAV vector

along with helper plasmids (pDJ and pHelper) by the calcium phosphate method. 72 hours post transfection, cells were harvested, nuclei lysed and virus purified over an iodixanol gradient column (2 hrs at 80K RPM in an S80AT3 rotor). Virus was dialyzed to remove excess iodixanol and aliquoted for injection.

Stereotactic injection of AAV

Stereotactic injection of P21 animals was previously described[20]. The localization and AAV expression were confirmed by the presence of GFP. The coordinates for P21 CA1 (hippocampus) injections are (A-P/M-L/D-V from Bregma): −3.2, ±3.5, −2.6. The coordinates for P21 granule cell (olfactory bulb) injections are (A-P/M-L/D-V from Bregma): +4.4, ±1.0, −1.5.

Buried food-finding assay

Animal behavior was performed as previously described[29]. Nrxn3α/β cKO male and female mice were stereotactically injected on P21 with AAV expressing GFP fused to inactive (control) or active (cre) cre-recombinase. On P60, the animals were singly housed for one week prior to the experiment. 18 hours before the start of the experiment, the animals were deprived of food to increase food-finding motivation. On the day of the experiment, the animals were acclimated to the testing room for 1hr. The mice were removed from their home cage and placed into a holding cage while a single food pellet was buried randomly in one of the corners. The mouse was returned to the home cage and the latency to food finding was measured. All trials were performed blind to the injection conditions and video recorded for post hoc analysis.

AMPAR surface labeling

GluA1 (1:4; Calbiochem, PC246) and GluA2 (1:100; Millipore, MAB397) surface labeling was performed as previously described[20,38]. Briefly, cultures were washed with PBS containing 0.5 mM $CaCl_2$ and 1 mM $MgCl_2$ (PBS^{MC}) with 4% sucrose. Neurons were preincubated at 37° C for 5 min with primary antibodies against GluA1 to allow labeling of surface AMPA receptors, washed with ice-cold PBS^{MC}, fixed with 4% PFA + 4% sucrose for 15 minutes, then blocked in a detergent-free blocking solution (PBS with 2% normal goat serum (Sigma, St. Louis, MO), and 0.02% sodium azide) for 1 hr, followed by secondary antibody incubation at room temp for 1 hour. To immunolabel for excitatory synaptic markers, cultures were then postfixed with –20°C methanol for 1 min to permeabilize the neurons. Cells were blocked in blocking solution for 1 hr, followed by incubation with primary antibodies for PSD95 (1:200; Pierce, 6G6-1C9) and VGluT1 (1:500; Millipore AB5905). Neurons were washed, then incubated with a secondary antibody at room temp for 1hr.

AMPAR internalization assays

The GluA1 internalization assay was essentially performed as previously described[20, 39]. Live hippocampal neurons at 14–16 days in vitro were labeled at 37°C for 5 min with a primary antibody against an extracellular epitope of GluA1 to allow labeling of surface AMPA receptors. Cells were washed in PBS^{MC} then incubated at 37°C with neuron growth

media for 15–20 minutes to allow for basal internalization. Cells were then washed and fixed with 4% PFA/4% sucrose, blocked in a detergent-free blocking solution for 1 hr, followed by an AlexaFluor488 secondary antibody incubation at room temp for 1hr to label the surface population. Neurons were then postfixed with 100% methanol at –20°C and stained with an AlexaFluor546 secondary antibody to immunolabel the pre-labeled internalized fraction. To calculate the percent internalization, the integrated red fluorescence intensity, identifying internalized GluA1, was divided by the total (red + green) intensity.

Olfactory bulb immunocytochemistry

Olfactory bulb cultures (DIV14-15) were fixed with 4% PFA + 4% sucrose, permeabilized with 0.02% Triton-X-100 in PBS (3×5′) and blocked for 1 hr in blocking solution. Fixed and permeabilized neurons were incubated with primary antibodies to detect Gephyrin (1:500; Synaptic Systems 147 003), vGAT (1:500; Synaptic Systems 131 011) and vGluT1. Cells were washed and stained with fluorescently conjugated secondary antibodies.

Image acquisition and quantifications

Image acquisition was performed previously[20,38,40]. Cells were chosen at random from three or more independent cultures. Images were taken from at least three coverslips per experiment. Fluorescent images were acquired at room temperature with an Olympus (Tokyo, Japan) FV1000 BX61WI laser-scanning confocal microscope using an Olympus Plan Apochromat 60× oil objective (NA: 1.42; WD: 0.15) set to 3× zoom with sequential acquisition, averaging of 3 frames, and set to 1024×1024 pixel resolution. Laser power and photomutiplier settings were set so bleed-through was negligible between channels. Within the same experiment, the same settings for laser power, PMT gain, and offset were used. These settings provided images where the brightest pixels were just under saturation. Digital images were taken using the Olympus Fluoview Imaging software (Olympus). 7–12 0.5 μm optical sections were used and maximum pixel intensity projections were created. Quantification of images was performed as previously described[20,38,40]. In brief, images were thresholded by intensity to exclude background signals and puncta were quantified by counting the number of puncta whose areas ranged from 0.1–4.0 μm^2. For each experiment, at least 15 cells per condition were analyzed and the mean and SEM were calculated. Data shown represent the average of the mean values from at least 3 independent experiments with each experiment consisting of the analysis of 12–20 cells per experimental condition. An experimenter blind to the conditions performed image-capture and quantification.

Quantitative immunoblotting was performed using ^{125}I secondary antibodies an imaged using a Typhoon Phosphoimager (GE Healthcare). Protein samples were either from adult littermate wild-type or constitutive Nrxn3α/β KO mice.

Statistics

The experimenter was blinded to all conditions during data collection and analysis. All values from culture electrophysiology experiments are represented by the average of independent experiments ± SEM with the exceptions being the paired-pulse ratio measurements in figures: 6e &f, 6i & 6j, 7e & 7f, 7h & i, 7j – m, in these experiments, the numbers represent the number of total cells recorded ± SEM. Acute slice experiments (Fig.

5c–f and 8d) are represented by the total number of cells per condition ± SEM. For the buried food-finding behavior (Fig. 8e), the total number of animals was used to determine the average latency ± SEM. No statistical methods were used to predetermine sample sizes, but our sample sizes are similar to those generally employed in the field. Data distribution was assumed to be normal but this was not formally tested, thus we have displayed individual data points for all 2-bar bar graphs. Statistical significance for electrophysiological and behavioral experiments was determined by single-factor ANOVA from a two-tailed test. Significance of weight distribution was determined by 2-way ANOVA. Statistical analysis of cumulative probabilities was tested by a Kolmogorov-Smirnov test (K-S test) from: http://www.physics.csbsju.edu/stats/KS-test.n.plot_form.html. A supplementary methods checklist is available.

Supplementary Material

Refer to Web version on PubMed Central for supplementary material.

Acknowledgments

We thank Drs. D. Martinelli, P. Rothwell, L. Chen and R.C. Malenka for advice and technical help. This study was supported by grants from the NIMH (R37MH52804 to T.C.S.), the NIDA (K99DA034029 to C.F.) and the A.H.A. (11POST7360078 to J.A.) and NIMH (NIMH: 1K99MH103531to J.A.).

References

1. Bang ML, Owczarek S. A matter of balance: role of neurexin and neuroligin at the synapse. Neurochem Res. 2013; 38:1174–1189.10.1007/s11064-013-1029-9 [PubMed: 23559421]
2. Knight D, Xie W, Boulianne GL. Neurexins and neuroligins: recent insights from invertebrates. Mol Neurobiol. 2011; 44:426–440.10.1007/s12035-011-8213-1 [PubMed: 22037798]
3. Krueger DD, Tuffy LP, Papadopoulos T, Brose N. The role of neurexins and neuroligins in the formation, maturation, and function of vertebrate synapses. Curr Opin Neurobiol. 2012; 22:412–422.10.1016/j.conb.2012.02.012 [PubMed: 22424845]
4. Südhof TC. Neuroligins and neurexins link synaptic function to cognitive disease. Nature. 2008; 455:903–911.10.1038/nature07456 [PubMed: 18923512]
5. Tabuchi K, Südhof TC. Structure and evolution of neurexin genes: insight into the mechanism of alternative splicing. Genomics. 2002; 79:849–859.10.1006/geno.2002.6780 [PubMed: 12036300]
6. Ushkaryov YA, et al. Conserved domain structure of beta-neurexins. Unusual cleaved signal sequences in receptor-like neuronal cell-surface proteins. J Biol Chem. 1994; 269:11987–11992. [PubMed: 8163501]
7. Ushkaryov YA, Petrenko AG, Geppert M, Südhof TC. Neurexins: synaptic cell surface proteins related to the alpha-latrotoxin receptor and laminin. Science. 1992; 257:50–56. [PubMed: 1621094]
8. Reichelt AC, Rodgers RJ, Clapcote SJ. The role of neurexins in schizophrenia and autistic spectrum disorder. Neuropharmacology. 2012; 62:1519–1526.10.1016/j.neuropharm.2011.01.024 [PubMed: 21262241]
9. Kim HG, et al. Disruption of neurexin 1 associated with autism spectrum disorder. Am J Hum Genet. 2008; 82:199–207.10.1016/j.ajhg.2007.09.011 [PubMed: 18179900]
10. Kirov G, et al. Neurexin 1 (NRXN1) deletions in schizophrenia. Schizophr Bull. 2009; 35:851–854.10.1093/schbul/sbp079 [PubMed: 19675094]
11. Sato N, et al. Association between neurexin 1 (NRXN1) polymorphisms and the smoking behavior of elderly Japanese. Psychiatr Genet. 2010; 20:135–136.10.1097/YPG.0b013e32833a21f9 [PubMed: 20414139]

12. Docampo E, et al. Association of neurexin 3 polymorphisms with smoking behavior. Genes Brain Behav. 2012; 11:704–711.10.1111/j.1601-183X.2012.00815.x [PubMed: 22716474]
13. Hishimoto A, et al. Neurexin 3 polymorphisms are associated with alcohol dependence and altered expression of specific isoforms. Hum Mol Genet. 2007; 16:2880–2891.10.1093/hmg/ddm247 [PubMed: 17804423]
14. Kelai S, et al. Nrxn3 upregulation in the globus pallidus of mice developing cocaine addiction. Neuroreport. 2008; 19:751–755.10.1097/WNR.0b013e3282fda231 [PubMed: 18418251]
15. Lachman HM, et al. Genomewide suggestive linkage of opioid dependence to chromosome 14q. Hum Mol Genet. 2007; 16:1327–1334.10.1093/hmg/ddm081 [PubMed: 17409192]
16. Novak G, Boukhadra J, Shaikh SA, Kennedy JL, Le Foll B. Association of a polymorphism in the NRXN3 gene with the degree of smoking in schizophrenia: a preliminary study. World J Biol Psychiatry. 2009; 10:929–935.10.1080/15622970903079499 [PubMed: 19658047]
17. Prats-Puig A, et al. Variations in the obesity genes FTO, TMEM18 and NRXN3 influence the vulnerability of children to weight gain induced by short sleep duration. Int J Obes (Lond). 2013; 37:182–187.10.1038/ijo.2012.27 [PubMed: 22391885]
18. Treutlein B, Gokce O, Quake SR, Südhof TC. Cartography of neurexin alternative splicing mapped by single-molecule long-read mRNA sequencing. Proc Natl Acad Sci U S A. 2014; 111:E1291–1299.10.1073/pnas.1403244111 [PubMed: 24639501]
19. Ullrich B, Ushkaryov YA, Südhof TC. Cartography of neurexins: more than 1000 isoforms generated by alternative splicing and expressed in distinct subsets of neurons. Neuron. 1995; 14:497–507. [PubMed: 7695896]
20. Aoto J, Martinelli DC, Malenka RC, Tabuchi K, Südhof TC. Presynaptic Nrxn3 alternative splicing trans-synaptically controls postsynaptic AMPA receptor trafficking. Cell. 2013; 154:75–88.10.1016/j.cell.2013.05.060 [PubMed: 23827676]
21. Missler M, et al. Alpha-neurexins couple Ca2+ channels to synaptic vesicle exocytosis. Nature. 2003; 423:939–948.10.1038/nature01755 [PubMed: 12827191]
22. Chen YC, et al. Drosophila neuroligin 2 is required presynaptically and postsynaptically for proper synaptic differentiation and synaptic transmission. J Neurosci. 2012; 32:16018–16030.10.1523/JNEUROSCI.1685-12.2012 [PubMed: 23136438]
23. Hu Z, et al. Neurexin and neuroligin mediate retrograde synaptic inhibition in C. elegans. Science. 2012; 337:980–984.10.1126/science.1224896 [PubMed: 22859820]
24. Fowler SC, et al. A force-plate actometer for quantitating rodent behaviors: illustrative data on locomotion, rotation, spatial patterning, stereotypies, and tremor. J Neurosci Methods. 2001; 107:107–124. [PubMed: 11389948]
25. Dobrunz LE, Stevens CF. Heterogeneity of release probability, facilitation, and depletion at central synapses. Neuron. 1997; 18:995–1008. [PubMed: 9208866]
26. Hessler NA, Shirke AM, Malinow R. The probability of transmitter release at a mammalian central synapse. Nature. 1993; 366:569–572.10.1038/366569a0 [PubMed: 7902955]
27. Murthy VN, Sejnowski TJ, Stevens CF. Heterogeneous release properties of visualized individual hippocampal synapses. Neuron. 1997; 18:599–612. [PubMed: 9136769]
28. Rosenmund C, Clements JD, Westbrook GL. Nonuniform probability of glutamate release at a hippocampal synapse. Science. 1993; 262:754–757. [PubMed: 7901909]
29. Cao P, Maximov A, Südhof TC. Activity-dependent IGF-1 exocytosis is controlled by the Ca(2+)-sensor synaptotagmin-10. Cell. 2011; 145:300–311.10.1016/j.cell.2011.03.034 [PubMed: 21496647]
30. Citri A, Pang ZP, Südhof TC, Wernig M, Malenka RC. Comprehensive qPCR profiling of gene expression in single neuronal cells. Nat Protoc. 2012; 7:118–127.10.1038/nprot.2011.430 [PubMed: 22193304]
31. Földy C, Malenka RC, Südhof TC. Autism-associated neuroligin-3 mutations commonly disrupt tonic endocannabinoid signaling. Neuron. 2013; 78:498–509.10.1016/j.neuron.2013.02.036 [PubMed: 23583622]
32. Iijima T, Iijima Y, Witte H, Scheiffele P. Neuronal cell type-specific alternative splicing is regulated by the KH domain protein SLM1. J Cell Biol. 2014; 204:331–342.10.1083/jcb.201310136 [PubMed: 24469635]

33. Iijima T, et al. SAM68 regulates neuronal activity-dependent alternative splicing of neurexin-1. Cell. 2011; 147:1601–1614.10.1016/j.cell.2011.11.028 [PubMed: 22196734]
34. Kaeser PS, et al. RIM proteins tether Ca2+ channels to presynaptic active zones via a direct PDZ-domain interaction. Cell. 2011; 144:282–295.10.1016/j.cell.2010.12.029 [PubMed: 21241895]
35. Maximov A, Pang ZP, Tervo DG, Südhof TC. Monitoring synaptic transmission in primary neuronal cultures using local extracellular stimulation. J Neurosci Methods. 2007; 161:75–87.10.1016/j.jneumeth.2006.10.009 [PubMed: 17118459]
36. Pang ZP, et al. Doc2 supports spontaneous synaptic transmission by a Ca(2+)-independent mechanism. Neuron. 2011; 70:244–251.10.1016/j.neuron.2011.03.011 [PubMed: 21521611]
37. Zhang C, et al. Neurexins physically and functionally interact with GABA(A) receptors. Neuron. 2010; 66:403–416.10.1016/j.neuron.2010.04.008 [PubMed: 20471353]
38. Aoto J, Nam CI, Poon MM, Ting P, Chen L. Synaptic signaling by all-trans retinoic acid in homeostatic synaptic plasticity. Neuron. 2008; 60:308–320.10.1016/j.neuron.2008.08.012 [PubMed: 18957222]
39. Lin JW, et al. Distinct molecular mechanisms and divergent endocytotic pathways of AMPA receptor internalization. Nat Neurosci. 2000; 3:1282–1290.10.1038/81814 [PubMed: 11100149]
40. Nam CI, Chen L. Postsynaptic assembly induced by neurexin-neuroligin interaction and neurotransmitter. Proc Natl Acad Sci U S A. 2005; 102:6137–6142.10.1073/pnas.0502038102 [PubMed: 15837930]

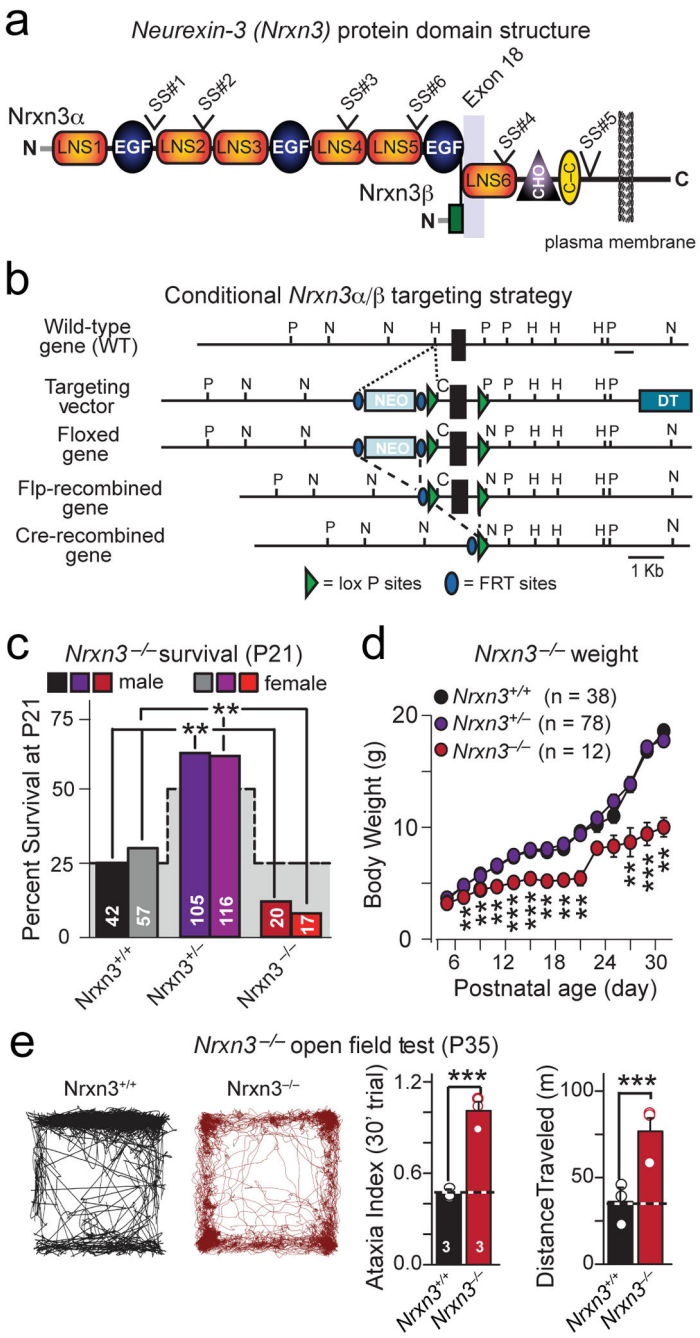

Figure 1. Generation of conditional and constitutive *Nrxn3α/β* KO mice: Constitutive *Nrxn3α/β* KO impairs survival

a, Structure of Nrxn3α and Nrxn3β, with locations of the six canonical sites of alternative splicing (SS#1 to SS#6) and of exon 18. LNS: Laminin G-neurexin-sex hormone binding globulin domain. EGF: Epidermal growth factor-like repeat. CHO: carbohydrate-attachment sequence. C-C: cysteine loop.

b, Targeting strategy for the generation of conditional *Nrxn3α/β* KO mice in which all Nrxn3α and Nrxn3β forms neurexins are conditionally deleted by cre-recombinase.

c, Survival rates of P21 of male and female offspring from heterozygous constitutive *Nrxn3α/β* KO mice (stepped background shadow = expected Mendelian ratio; p<0.001).
d, Average body weight of $Nrxn3^{+/+}$, $Nrxn3^{+/-}$ and $Nrxn3^{-/-}$ mice as a function of age (P5: p = 0.144; P7: p = 0.00375; P9: = 0.003; P11: p = 0.00134; P13: p < 0.0001; P15: p < 0.0001; P17: p = 0.0001; P19: p = 0.000178; P21: p = 0.0151; P23: p = 0.305; P25: p = 0.0807; P27: p = 0.0115; P29: p < 0.0001; P31: p = 0.00999).
e, Distance moved (left) and ataxia indices (right) of P35 *Nrxn3α/β* KO mice over a 30 min force plate trial (***, p <0.0001).
Data shown in (**d** and **e**) are means ± SEMs (numbers in bars = number of mice analyzed. Statistical significance was assessed using the χ^2-test comparing the observed to the expected Mendelian distribution (**c**) or by single-factor ANOVA (**d** and **e**). For additional information see supplementary figure 1.

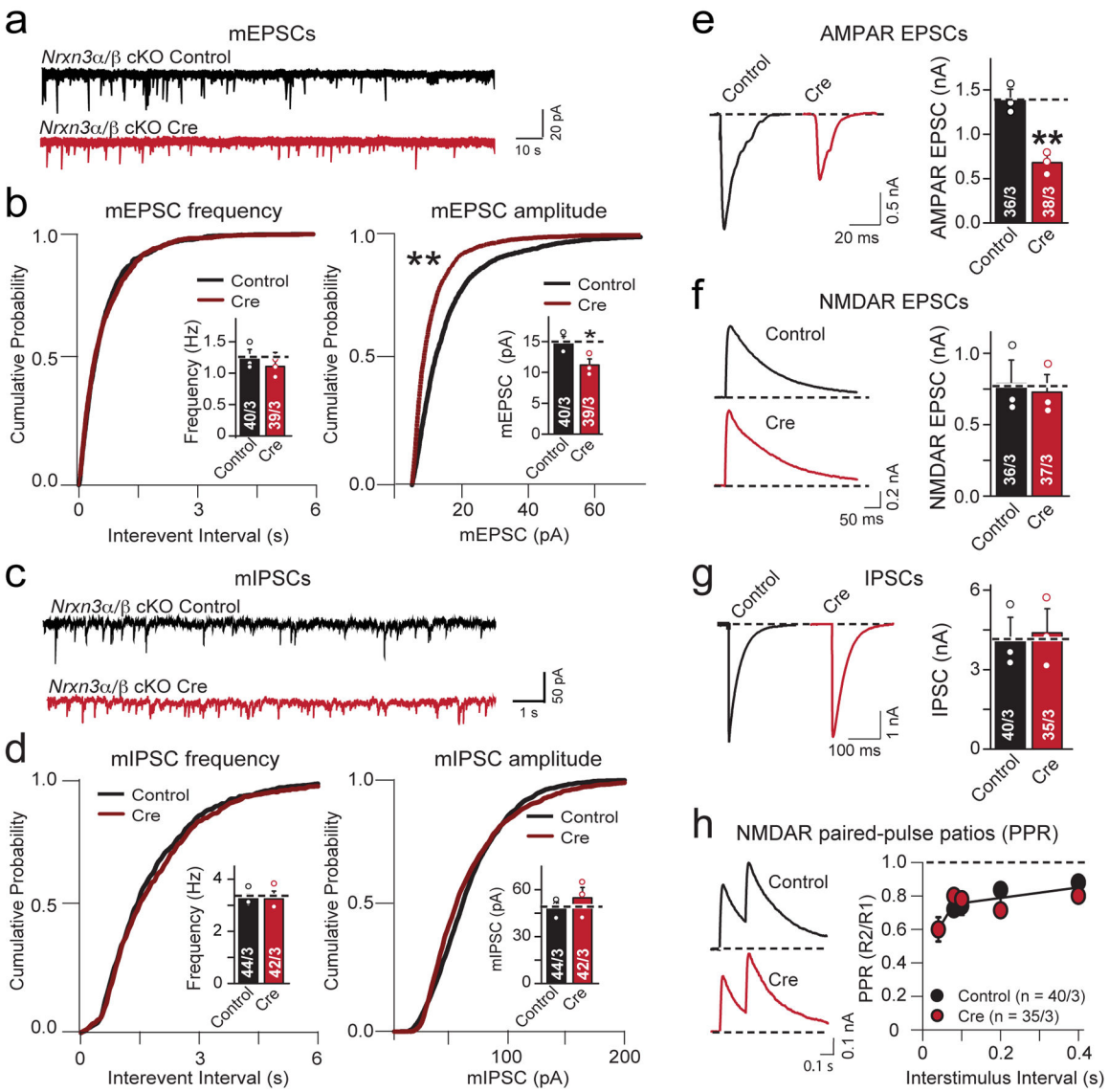

Figure 2. Conditional *Nrxn3α/β*KO selectively decreases AMPAR-mediated synaptic transmission in cultured hippocampal neurons

a, Representative traces of mEPSCs recorded from cultured hippocampal pyramidal neurons from homozygous *Nrxn3α/β* cKO mice in 1 μM tetrodotoxin and 100 μM picrotoxin. Neurons were infected with lentiviruses expressing inactive (control) or active cre-recombinase (cre) at 4–5 days in vitro (DIV), and analyzed at 14–16 DIV.

b, Cumulative distribution plots of the mEPSC frequency and amplitude in hippocampal Nrxn3α/β cKO neurons infected with lentiviruses expressing inactive (control) or active cre-recombinase (cre) (mEPSC frequency cumulative probability: $p = 0.972$, frequency: $p = 0.128$; amplitude cumulative probability: $p < 0.0001$, mEPSC amplitude bar graph: $p = 0.0216$).

c & **d,** Same as in **a** & **b**, but analyzing mIPSCs (mIPSC frequency cumulative probability: $p = 0.481$, frequency: $p = 0.879$; amplitude cumulative probability: $p = 0.392$, amplitude: $p = 0.467$).

e–g, Evoked synaptic responses in control and *Nrxn3α/β* cKO neurons. Panels show representative traces (left) and summary graphs of the response amplitudes (right) for AMPAR- (**e**; p = 0.0036) and NMDAR-mediated EPSCs (**f**; p = 0.752) and for GABA-receptor-mediated IPSCs (**g**; p = 0.821).

h, Paired-pulse ratio measurements of NMDAR-mediated EPSCs demonstrate that there is no change in release probability in Nrxn3α/β deficient neurons (80 ms ISI: p = 0.969)

Data shown are means ± SEM; numbers of cells/independent cultures analyzed are indicated. Statistical significance was assessed by K-S test for cumulative probability plots, (**b** and **d**) and single-factor ANOVA. For more information, please supplementary figure 2.

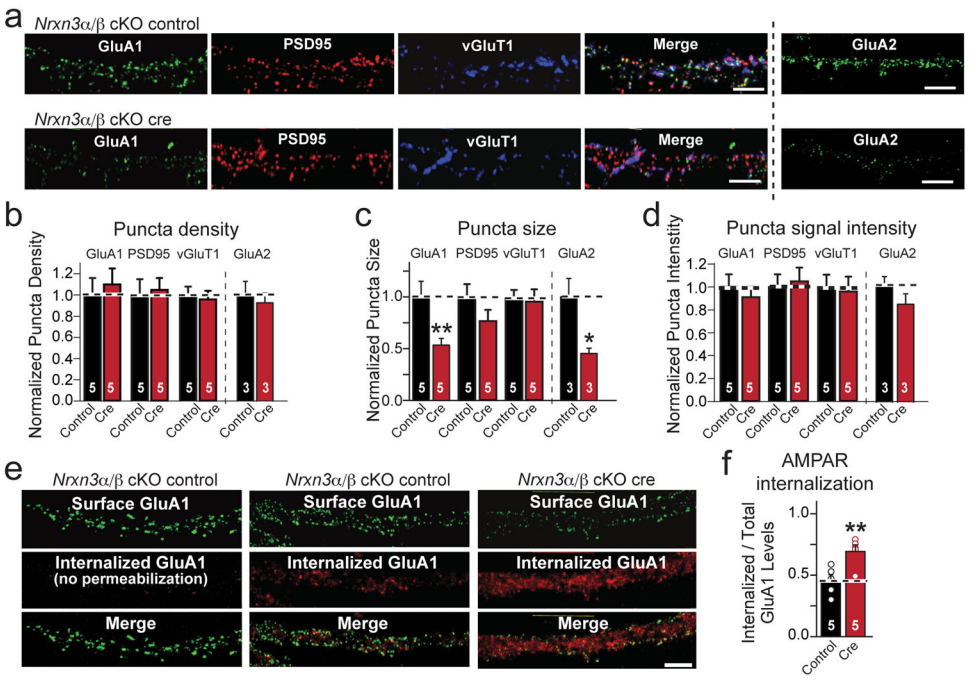

Figure 3. Conditional *Nrxn3α/β* KO destabilizes postsynaptic AMPAR-levels

a, Representative immunofluorescence images of dendritic surface-exposed AMPA-receptor subunits GluA1 and GluA2 and of synaptic markers vGluT1 and PSD95 in control and *Nrxn3α/β* cKO neurons (scale bar = 5 μm).

b–d, Density (**b**), size (**c**), and intensity (**d**) of GluA1-, GluA2-, PSD95-, and vGluT1-containing synapses in control and *Nrxn3α/β* cKO neurons (Density: GluA1, p = 0.698; GluA2, p = 0.631; PSD95, p = 0.818; vGluT1, p = 0.758. Size: GluA1, p = 0.018; GluA2, p = 0.0387, PSD95, p = 0.186; vGluT1, p = 0.421. Intensity: GluA1, p = 0.579; GluA2, p = 0.267; PSD95, p = 0.821; vGluT1, p = 0.796).

e–f, Representative images (**e**) and summary graph (**f**) of GluR1 internalization experiments in which control and *Nrxn3α/β* KO neurons were incubated with GluA1 antibodies for 5 min, chased for 20 min, and then the surface-exposed and internalized GluR1 was labeled with two different secondary antibodies. Control images on the left are from neurons without permeabilization to ensure that surface-exposed and internalized GluA1 can be cleanly differentiated (scale bar = 5 μm). Internalization is quantified (**f**) as the ratio of internalized to total GluA1 (**, p = 0.0034).

Data in **b–d** and **f** are means ± SEM (n=5 cultures); statistical significance was evaluated by single factor ANOVA. Please see supplementary figure 3 for absolute quantification of puncta parameters.

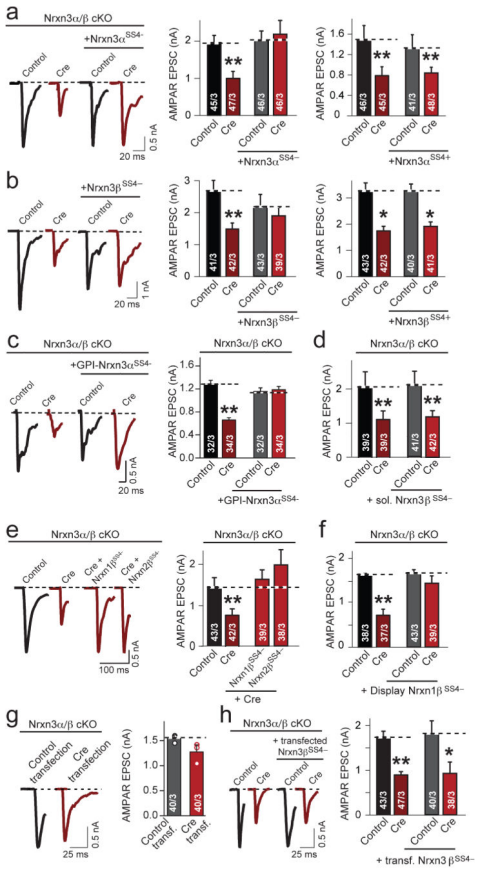

Figure 4. Rescue of AMPAR-mediated EPSCs in cultured hippocampal *Nrxn3α/β* cKO neurons by pre-synaptic neurexins lacking an insert in SS#4

a–f, Summary data of AMPAR-mediated EPSC rescue experiments, performed as in Figure 2a and co-infected with lentivirus expressing the following:

a, Nrxn3α^{SS4-} (cre: p = 0.0014; cre + Nrxn3α^{SS4-}: p = 0.962) or Nrxn3α^{SS4+} (cre: p = 0.00836; cre + Nrxn3α^{SS4+}: p = 0.00450).

b, Nrxn3β $^{SS4-}$ (cre: p = 0.00785; cre + Nrxn3β^{SS4-}: p = 0.647) or Nrxn3β^{SS4-} (cre: p = 0.0138; cre + Nrxn3β^{SS4+}: p = 0.0118).

c, GPI-Nrxn3α^{SS4-} (cre: p = 0.0009; cre + GPI-Nrxn3α^{SS4-}: p = 0.742).

d, Endogenous soluble form of *Nrxn3β^{SS4-}* (cre: p = 0.003; cre + sNrxn3β^{SS4-}: p = 0.007).

e, Nrxn1β^{SS4-} and *Nrxn2β^{SS4-}* (cre: p = 0.0025; cre + *Nrxn1β^{SS4-}*: p = 0.717; cre + *Nrxn2β^{SS4-}*: p = 0.697).

f, Nrxn1β^{SS4-} fused to the PDGF receptor (cre: p = 0.0073; cre + Nrxn1β^{SS4-}-PDGFR: p = 0.535).

g, Traces and summary graph of AMPAR-mediated EPSCs measured in GFP-positive *Nrxn3α/β* cKO neurons sparsely co-transfected with inactive (control) or active cre-recombinase (cre) and EGFP (p = 0.100).

h, Traces and summary graph of AMPAR-mediated EPSCs measured in GFP+ *Nrxn3α/β* cKO neurons, infected with lentivirus (as in (**a**)), and sparsely co-transfected with EGFP and Nrxn3β^{SS4-},plasmids (**, p = 0.00112; *, p = 0.0186).

Data shown are means ± SEMs; numbers in bars: cells/independent cultures analyzed. Statistical significance was assessed using single-factor ANOVA. For more information, please see supplementary figure 4.

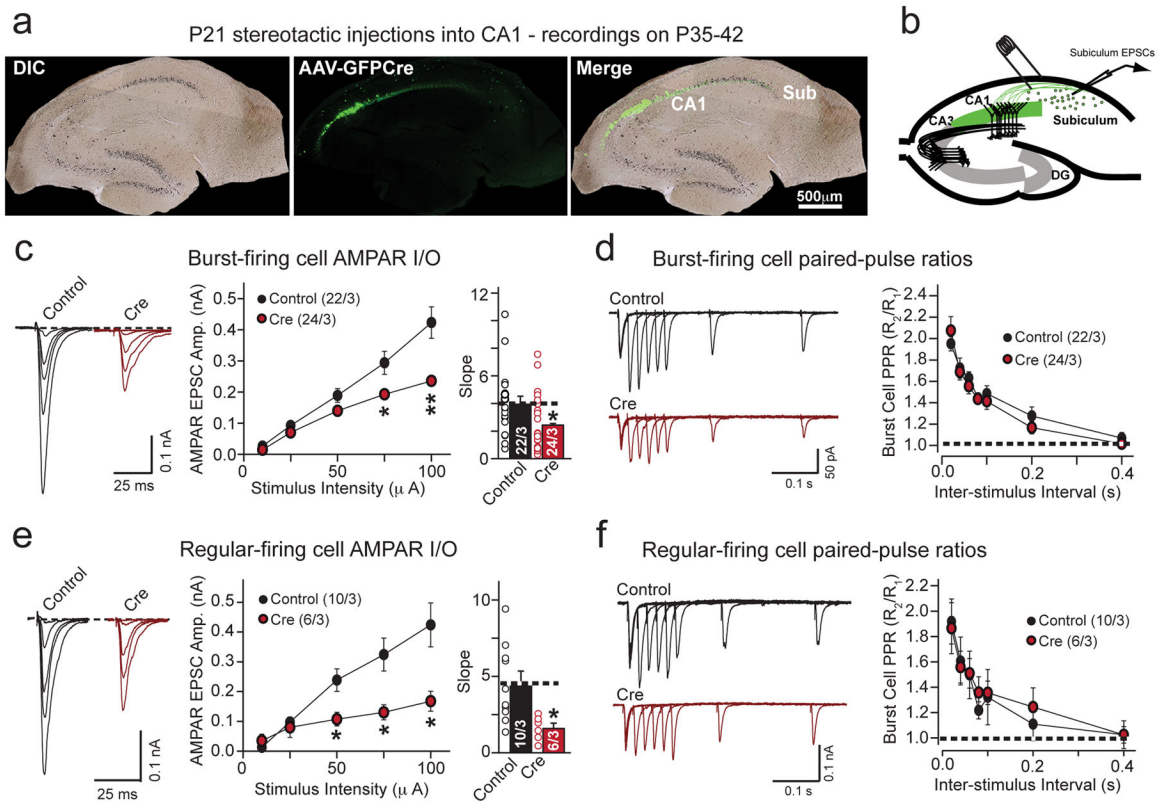

Figure 5. Conditional *in vivo* ablation of *Nrxn3α/β* in presynaptic hippocampal CA1-region neurons impairs postsynaptic AMPAR-mediated responses in the subiculum

a, Hippocampal brain sections of P35 male animals illustrating complete targeted infection of the CA1-region without significant infection of the subiculum, following the stereotactic injection of AAVs expressing EGFP-tagged inactive (control) or active (cre) cre-recombinase at P21 (scale bar: 500 μm).

b, Schematic illustrating the electrophysiological recording configuration to selectively evoke AMPAR-mediated EPSCs at CA1-subiculum synapses.

c & e, Input-output representative traces (left), summary graph (middle) and slope (right) for AMPAR EPSCs measured in burst spiking (**c**; 10μA: p = 0.0728; 25μA: p = 0.177; 50μA: p = 0.122; 75μA: p = 0.0198; 100μA: p = 0.00748 and slope: p = 0.0362) or regular spiking (**e**; 10μA: p = 0.132; 25μA: p = 0.188; 50μA: p = 0.0248, 75μA: 0.0349, 100μA: 0.035 and slope: p = 0.0172) neurons from mice prepared as in (**a**).

d & f, Paired-pulse ratio measurements from burst spiking **(d**; 60ms ISI: p = 0.422**)** or regular spiking **(f**; 60ms ISI: p = 0.954**)** subicular neurons in mice injected with inactive (control) or active (cre) cre-recombinase in region CA1. Representative traces (left) and summary graph (right) are shown.

Data are means ± SEMs; means were calculated from the total number of cells. Numbers in bars: cell/animal. Statistical significance was assessed using single-factor ANOVA. For more information on subicular neuron identification and passive membrane properties of each cell type, see supplementary figure 5.

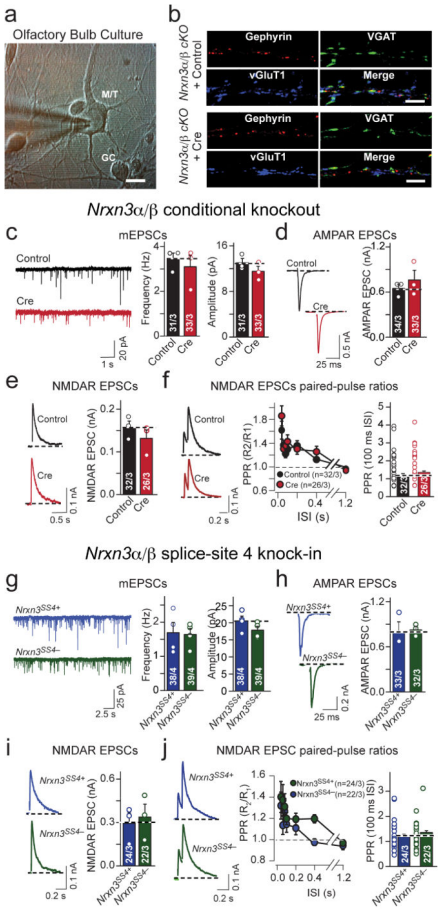

Figure 6. Different from the hippocampus *Nrxn3α/β* is not required for AMPAR-mediated synaptic responses in the olfactory bulb

a, Representative image of DIV 14 cultured olfactory bulb neurons. Note the difference in soma size that was used to identify neuron subtypes (M/T: mitral/tufted cell; GC: granule cell; scale bar: 10 μm).

b, Representative images of excitatory and inhibitory synapse density immunostained for inhibitory (vGAT and gephyrin) and excitatory (vGluT1) markers in cultured *Nrxn3α/β* cKO olfactory bulb neurons infected with lentiviruses expressing EGFP-tagged inactive (control) or active (cre) cre-recombinase. n = 3 experiments; scale bar: 5 μm.

c–f, Sample traces and summary graphs of mEPSCs (**c**; frequency: p = 0.603; amplitude: p = 0.276), AMPAR EPSCs **(d**; p = 0.469**)**, NMDAR EPSCs **(e**; p = 0.537**)** and NMDAR paired-pulse ratios (**f**; 100ms ISI: p = 0.300) recorded from *Nrxn3α/β* cKO mitral/tufted olfactory bulb neurons, cultured as in (**b**).

g–j, Sample traces and summary graphs of mEPSCs (**g**; frequency: p = 0.883; amplitude: p = 0.181), evoked AMPAR EPSCs (**h**; p = 0.881), evoked NMDAR EPSCs (**i**; p = 0.721) and NMDAR-EPSC paired-pulse ratios (**j**; 100ms ISI: 0.807) recorded from *Nrxn3α/β* SS#4 KI M/T olfactory bulb neurons infected with lentiviruses expressing EGFP-tagged inactive (*Nrxn3α/β*$^{SS4+}$) or active (*Nrxn3α/β*$^{SS4-}$) cre-recombinase.

Data are means ± SEM. Bar graphs: cells/ independent culture experiments. Means and SEMs: from three independent experiments except for figures **f** and **j**, where the number of

cells was. Statistical significance was determined by single-factor ANOVA. For more information, please see supplemental figure 6.

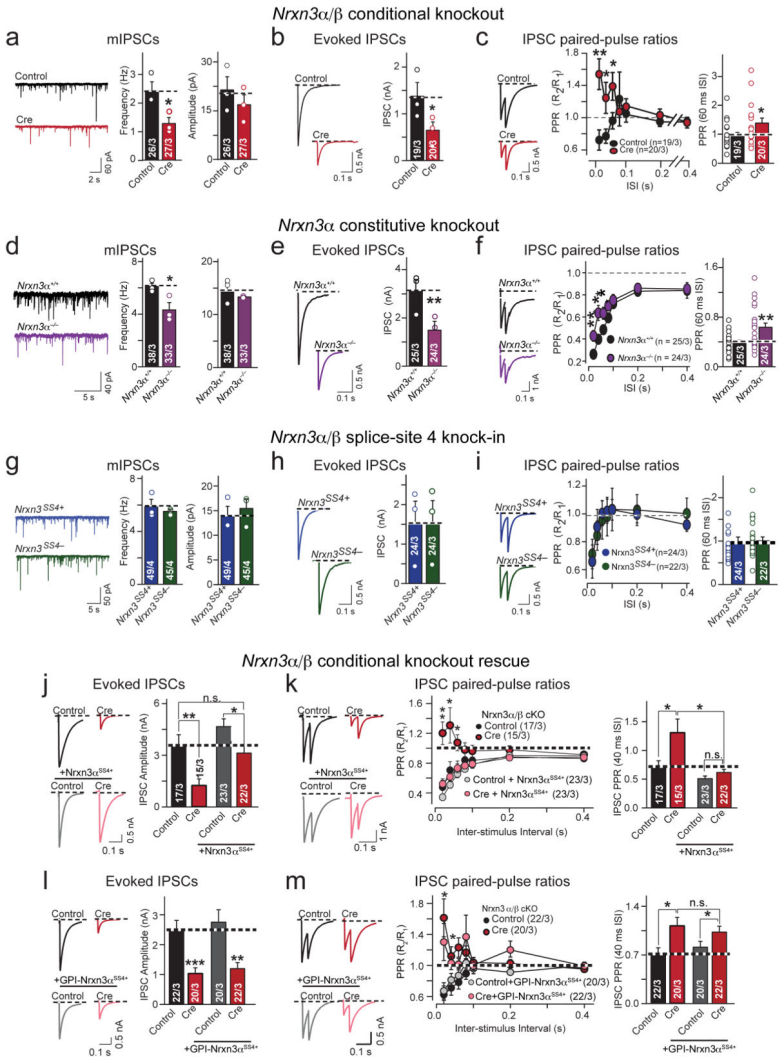

Figure 7. Nrxn3 is essential for presynaptic GABA release in olfactory bulb neurons by an SS#4-independent mechanism

a–c, Sample traces and summary graphs for mIPSCs (**a**; frequency: p = 0.039; amplitude: 0.419), evoked IPSCs (**b**; p = 0.024) and IPSC PPRs (**c**; p = 0.00264 (20ms ISI), 0.0365 (40ms), 0.450 (60ms)), recorded from mitral/tufted cells in cultured *Nrxn3α/β* cKO olfactory bulb neurons infected with lentiviruses expressing EGFP-tagged inactive (control) or active (cre) cre-recombinase

d–f, Same as (**a–c**), but measured in cultured *Nrxn3α*$^{+/+}$ and *Nrxn3α*$^{-/-}$ olfactory bulb neurons. (**d:** frequency: p = 0.0435; amplitude: p = 0.367; **e:** p = 0.0005; **f**: p = 0.00805 (20ms ISI), 0.00744 (40ms), 0.0327 (60ms)).

g–i, Same as (**a–c**), but measured in cultured *Nrxn3α/β* SS#4 KI olfactory bulb neurons (**g**: frequency: p = 0.536, amplitude: p = 0.614; **h**: p = 0.983; **i**: 60 ms ISI: p = 0.130). Neurons were infected with lentiviruses as in Fig. 6g[20].

j & k, Rescue of the GABAergic transmission in *Nrxn3α/β* cKO neurons by full-length Nrxn3α^{SS4+}. Evoked IPSC (**j**; cre: p = 0.0034; cre + Nrxn3α^{SS4+}: p = 0.0217) and IPSC PPRs (**k;** cre: p = 0.000515 (20ms ISI), 0.0363 (40ms), 0.02891 (60ms), cre + Nrxn3α^{SS4+}:

p = 0.0334 (20ms), 0.128 (40ms), 0.284 (60ms)) in mitral/tufted cells as in Fig. 7c, with or without full-length Nrxn3α^{SS4+}.

l & **m**, Same as in (**j**) and (**k**) but with a GPI-anchored Nrxn3α^{SS4+}. Evoked IPSCs (**l;** cre: p < 0.001; cre + GPI-Nrxn3α^{SS4+}: p = 0.00165) and IPSC PPRs (**m;** cre: p = 0.0006 (20ms ISI), 0.0107 (40ms), 0.0055 (60ms); cre + GPI-Nrxn3α^{SS4+}: p = 0.0231 (20ms), 0.0213 (40ms), ISI: 0.219 (60ms).

Data shown are means ± SEMs; the number of cells/independent cultures analyzed are indicated in the bars. Statistical analyses were calculated from the number of independent cultures (for **a**, **d** and **g**) and from cell number (**b**, **e**, **h**, **j–m**). Statistical significance was assessed using single-factor ANOVA. For more information, see supplementary figure 7.

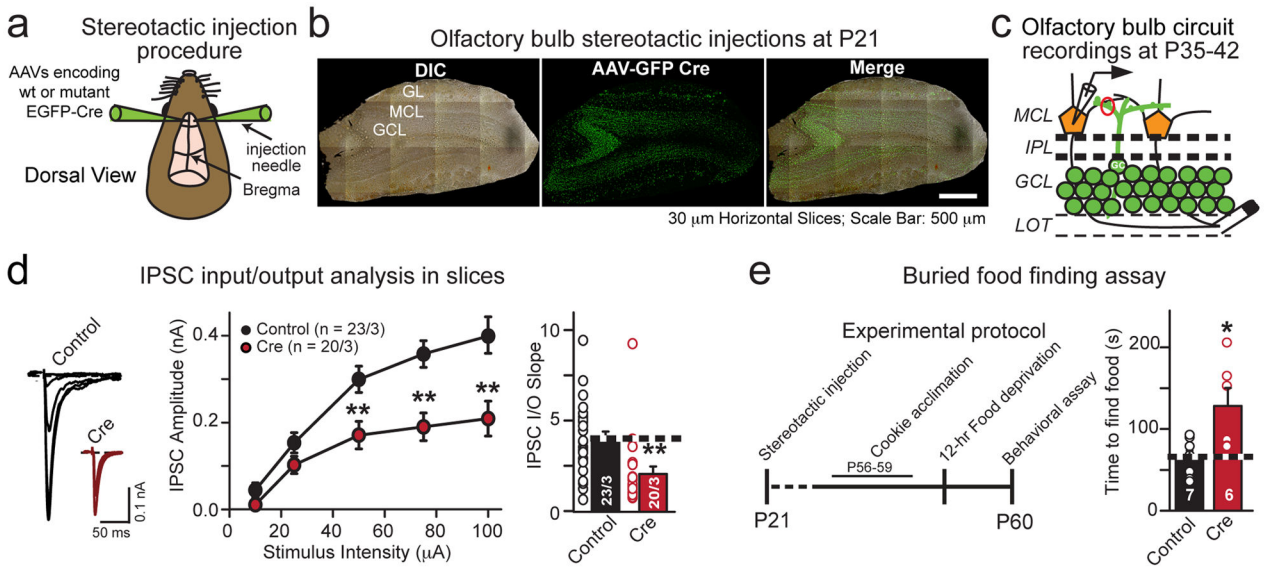

Figure 8. Conditional *in vivo* deletion of Nrxn3α/β in the olfactory bulb decreases GABAergic synaptic transmission at granule cell-mitral/tufted cell synapses and impairs an olfactory behavior

a, Schematic of bilateral stereotactic injections *in vivo* into the olfactory bulb.

b, Representative images of horizontal (30 μm) sections showing. complete infection of the granule cell layer. *Nrxn3α/β* cKO mice were bilaterally injected with AAV expressing EGFP fused to inactive (control) or active (cre) cre-recombibase at P21, and analyzed at P35-42. (scale bar: 500 μm).

c, Schematic of recording configuration from uninfected postsynaptic mitral/tufted cells in the mitral cell layer (MCL). Granule cell IPSCs were evoked by antidromic extracellular stimulation in the lateral olfactory tract (LOT).

d, IPSC input-output representative traces (left), plotted data (middle) and slope (right) from olfactory bulb slices from *Nrxn3α/β* cKO mice that had been infected as in (**b**). 10 μA: p = 0.0749; 25μA: p = 0.111; 50 μA: p = 0.00578; 75 μA: p = 0.00052; 100 μA: p = 0.0026; slope: p = 0.00370.

e, Schematic of the experimental protocol (left) and summary graph (right) of the buried food finding assay. Bilateral genetic ablation of *Nrxn3α/β* in olfactory bulbs (as in (**b**)) significantly increased the latency of food finding in behaving mice (p = 0.0162).

Data are means ± SEMs; the number of cells/independent animals analyzed are indicated in the bars (**d)** or number of animals (**e**). Statistical significance was assessed using single-factor ANOVA. For more information, see supplementary figure 8.